JCTC Journal of Chemical Theory and Computation

Article

pubs.acs.org/JCTC

State-of-the-Art Calculations of Sublimation Enthalpies for Selected Molecular Crystals and Their Computational Uncertainty

Ctirad Červinka* and Michal Fulem

Department of Physical Chemistry, University of Chemistry and Technology, Prague, Technická 5, CZ-166 28 Prague 6, Czech Republic

Supporting Information

ABSTRACT: A computational methodology for calculation of sublimation enthalpies of molecular crystals from first principles is developed and validated by comparison to critically evaluated literature experimental data. Temperature-dependent sublimation enthalpies for a set of selected 22 molecular crystals in their low-temperature phases are calculated. The computational methodology consists of several building blocks based on high-level electronic structure methods of quantum chemistry and statistical thermodynamics. Ab initio methods up to the coupled clusters with iterative treatment of single and double excitations and perturbative triples correction with an estimated complete basis set description [CCSD(T)/CBS] are used to calculate the cohesive energies of crystalline phases within a fragment-based additive scheme. Density functional theory (DFT) calculations with periodic boundary conditions (PBC) coupled with the quasi-harmonic approximation are used to evaluate the thermal contributions to the enthalpy of the solid phase. The properties of the vapor phase are calculated within the ideal-gas model using the rigid-rotor harmonic-oscillator model with correction for internal rotation using a one-dimensional hindered rotor approximation and a proper treatment of the molecular rotational degrees of freedom in the vicinity of 0 K. All individual terms contributing to the sublimation enthalpy as a function of temperature are discussed and their uncertainties estimated by comparison to critically evaluated experimental data.

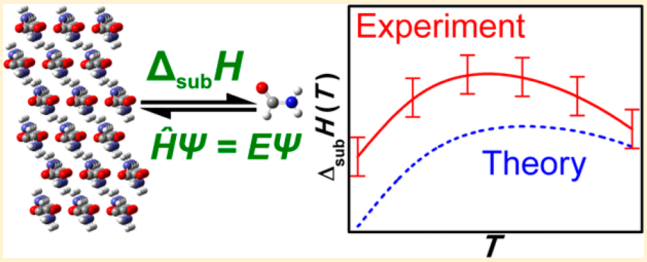

1. INTRODUCTION

Sublimation enthalpy ($\Delta_{sub}H$) is a key quantity representing the solid−vapor equilibrium below the triple point (coexistence of solid, liquid, and vapor phases) and the stability of the crystal structure the understanding and accurate description of which are indispensable for many applications including, for example, epitaxial technologies, crystal engineering, separation and purification techniques, pharmaceutical research, environmental modeling, and investigation of cosmic bodies. Sublimation enthalpy is also a key quantity for thermochemical calculations and correlations of solvation energies and enthalpies of formation in the gas phase. Experimental determinations of $\Delta_{sub}H$ for compounds exhibiting low volatility are very difficult, costly, and time-consuming.[1−3] Usually the interlaboratory agreement on experimental data for sublimation properties of low-volatility species is rather poor.[4−6] Moreover, empiric and semiempiric estimative methods for predictions based, for example, on the quantitative structure−property relationship (QSPR) models are not generally reliable or purely predictive, although effort is still exerted in this area.[7,8] On the other hand, the rapid increase of the number of known chemical species and the corresponding resolved crystal structures do not correlate with the amount of available experimental data on $\Delta_{sub}H$; typically, sublimation data are known for thousands of compounds, while millions of crystal structures have been resolved.[9] Therefore, a reliable and generally applicable computational methodology capable of predicting $\Delta_{sub}H$ from first principles would certainly find many uses in the future.

From a theoretical chemist's point of view, $\Delta_{sub}H$ has become an important quantity, possessing information about the cohesive properties of crystals. Since the cohesive (or lattice) energy (E^{cr}_{coh}) is not a directly experimentally accessible property, its calculated values cannot be simply compared to their experimental counterparts. For this purpose, a measurable property being in the closest relationship to the cohesive energy of a molecular crystal is $\Delta_{sub}H$. Therefore, data on $\Delta_{sub}H$ serve as a valuable benchmark for comparing and estimating the uncertainty of the values of E^{cr}_{coh} calculated by means of quantum chemistry. The E^{cr}_{coh} of a given crystalline phase reflects the intermolecular interactions in the crystalline phase and is the dominant contribution to $\Delta_{sub}H$.[10] Accurate computations of E^{cr}_{coh} are crucial for reliable predictions of the crystal structures, understanding the molecular aggregation during the nucleation and crystal growth processes, polymorph screening in pharmaceutical research,[11] and in the prediction of physical and thermodynamic properties of materials.[12−15] E^{cr}_{coh} can be computed from first principles either by a fragment-based additive approach or by calculations with periodic boundary conditions.[16−21]

Received: February 15, 2017
Published: April 24, 2017

DOI: 10.1021/acs.jctc.7b00164
J. Chem. Theory Comput. 2017, 13, 2840−2850

In our previous work,[17] ab initio fragment-based additive calculations of the cohesive energies and the uncertainty of such calculations were investigated and discussed in detail. From a comparison of calculated E_{coh}^{cr} values available in the literature, included in Table 4 in ref 17, it can be seen that the difference of E_{coh}^{cr} values for the same crystal calculated using various ab initio or DFT methods can amount to a few tens of percent. While quantum calculations with periodic boundary conditions for molecular crystals are limited to the density functional theory methods relying mostly on semiempirical correction for dispersion interactions, such as the DFT-D3 method by Grimme's group,[22] or to more advanced local second-order Møller–Plesset perturbation theory (LMP2)[23] in terms of the computational cost, fragment-based calculations can benefit from using a broad range of ab initio methods applicable to molecular clusters and from the availability of systematic improvement of the computational model by gradual inclusion of higher-order terms in the expansion.[20] On the other hand, in the desired region of the sub-kJ·mol^{-1} accuracy of the cohesive energies, some coincidental compensation of errors can occur and make the tight convergence of the cohesive energies less straightforward.[24] To overcome the weak points of both periodic and many-body expansion methods, several computational methodologies combining many-body expansion calculations in the short-range region with either periodic ab initio[25] or classical force-field calculations[16,24] were developed.

Our previous study[17] and several other groups[26−29] showed that MP2- and DFT-D3-based calculations predominantly yielded overestimated E_{coh}^{cr} results when compared to their CCSD(T) analogues, commonly accepted as the gold standard for computational data.[30] The effect of extrapolations toward the complete basis set (CBS)[31] typically amounts to 10% of the total E_{coh}^{cr}, which makes the CBS extrapolations a very important feature of all high accuracy calculations of E_{coh}^{cr}.[17,19,20,32] Using the fragment-based approaches, it turns out to be important to include some of the multibody interaction terms (typically three-body terms).[20]

Thermal properties of the crystalline phase are in principle accessible via both periodic or fragment-based calculations as well.[32,33] Basically, the density of phonon states is the key quantity required for evaluation of the thermal and zero-point vibrational energy terms. To account for the thermal expansion, it proves to be essential to follow the quasi-harmonic approximation.[34] Since these terms are expected to play a rather minor role in the total sum of $\Delta_{sub}H$, when compared to E_{coh}^{cr}, lowering the computational cost of such calculations, even if bringing a slight loss of accuracy, seems to be legitimate in this case. Therefore, dispersion-corrected DFT calculations are commonly accepted as sufficient for phonon calculations of the solid phase.

It is a rather straightforward task to calculate the thermodynamic properties of the vapor phase, assumed to behave ideally, by taking into account the extremely low vapor pressures of molecular crystals at considered temperatures, typically below 100 K, even though several important phenomena need to be considered with caution. First, the presence of any large-amplitude anharmonic internal degrees of freedom causes a need for a special treatment exceeding the basic rigid rotor–harmonic oscillator model (RRHO).[35] The one-dimensional hindered rotor model (1D-HR) has been proved to successfully describe the internal rotations.[36] Next, the extrapolation of $\Delta_{sub}H$ down to the temperatures close to 0 K requires a more careful approach to evaluate ideal-gas heat capacities ($C_p^{g,0}$) than simply using the high-temperature limit for the rotational and translational degrees of freedom due to the fact that several quantum effects cannot be neglected in this low-temperature region.[37] All these effects have been taken into account in this work and are discussed in the following sections.

This work presents the results of the development, extensive validation, and detailed testing of a computational methodology capable of reliably calculating $\Delta_{sub}H$ as a function of temperature. For this purpose, a test set of 22 simple molecular crystals with known experimental thermodynamic and structural data has been chosen. Our test set contains crystals exhibiting various bulk and molecular properties, including rare gases (neon, argon), nonpolar hydrocarbons (ethane, ethene, ethyne, propane, butane), solidified elemental gases (nitrogen, fluorine), polar-bond-containing molecules (formaldehyde, carbon dioxide, dimethyl ether), and a list of hydrogen-bonded crystals (ammonia, hydrogen peroxide, hydrogen fluoride, methanol, aminomethane, hydrazine, methylhydrazine, formic acid, formamide, and acetic acid). Calculated $\Delta_{sub}H$ data are confronted with literature experimental data the uncertainties of which have been critically evaluated in our laboratory.[17]

When compared to a single calculation of the static cohesive energy, rigorous evaluation of the thermal contributions to the thermodynamic properties of the crystalline phases represents a significantly more complex and costly task, typically on a par with the complexity of calculation of the Hessian of the total cohesive energy. Therefore, it was a common practice in the past to mimic the thermodynamic properties at finite temperatures and pressures using only the static cohesive energies corresponding to the absolute zero. This could not be a viable approach in a long-term perspective, since it neglects all thermal and entropic contributions, as emphasized in several recent publications.[12−14,32,38]

The novelty of our computational approach to calculate $\Delta_{sub}H$ consists of combining high-level ab initio calculated cohesive energies, properly treated thermal properties of the solid phase using DFT calculations and the quasi-harmonic approximation, and a rigorous treatment of the thermodynamic properties of the ideal-gas vapor phase even at very low temperatures. This way represents a highly consistent theoretical methodology the reliability of which is assessed by comparison with critically evaluated experimental data and their estimated uncertainties.

2. COMPUTATIONAL METHODS

Sublimation enthalpy ($\Delta_{sub}H$) is the difference of the enthalpies of the vapor phase (H^g) and the crystalline phase (H^{cr}). Assuming there is no solid–solid phase transition between 0 K and a temperature T, $\Delta_{sub}H(T)$ can be written as

$$\begin{aligned}\Delta_{sub}H(T) &= H^{g}(T) - H^{cr}(T)\\ &= -E_{coh}^{cr} + \Delta_{geom}^{cr\rightarrow g}E + \Delta_{ZPE}^{cr\rightarrow g}E + \Delta_{th,mol}^{cr\rightarrow g}E\\ &\quad - H_{th,mol}^{lattice} + H_{ro\text{-}tr}^{g}\end{aligned} \quad (1)$$

where E_{coh}^{cr} stands for the cohesive energy of the crystal at 0 K, $\Delta_{geom}^{cr\rightarrow g}E$ represents the energy change associated with the relaxation of a molecule in its crystal phase geometry to the geometry of an isolated molecule in the vapor phase, and $\Delta_{ZPE}^{cr\rightarrow g}E$ and $\Delta_{th,mol}^{cr\rightarrow g}E$ represent the energy differences between the vapor and crystal phase zero-point vibration energy and intramolecular contributions to thermal enthalpy, respectively. $H_{therm}^{lattice}$ is the thermal contribution of the intermolecular (lattice)

DOI: 10.1021/acs.jctc.7b00164
J. Chem. Theory Comput. 2017, 13, 2840−2850

vibrational modes, relevant only for the crystal phase. Note that the $H^{\text{lattice}}_{\text{therm}}$ term accounts also for the change of the cohesive energy related to the thermal expansion of the crystal lattice. $H^{\text{g}}_{\text{ro-tr}}$ is the contribution from the rotation and translation modes and the expansion work term of the vapor-phase molecules (at the high-temperature limit $H^{\text{g}}_{\text{ro-tr}} = 4RT$ for nonlinear molecules, $H^{\text{g}}_{\text{ro-tr}} = {}^{7}/_{2}RT$ for linear molecules, and $H^{\text{g}}_{\text{ro-tr}} = {}^{5}/_{2}RT$ for monatomic gases).

2.1. Cohesive Energies. Cohesive energies of the studied crystals were calculated in our previous work[17] using a fragment-based additive scheme (FBAS), in which $E^{\text{cr}}_{\text{coh}}$ values were calculated as a sum of intermolecular two-body and three-body interactions. Molecular pairs and triplets separated by no more than a cutoff distance (set to 9 Å) were treated quantum chemically, while more distant molecular pairs were treated classically as a system of electrostatic point charges yielding a corresponding long-range Coulomb interaction sum, neglecting polarizability effects. The symmetry of the crystal lattice was taken into account to decrease the number of molecular clusters treated quantum chemically.[39] In this work, $E^{\text{cr}}_{\text{coh}}$ data calculated using counterpoise-corrected B3LYP-D3,[22,40,41] MP2, and CCSD(T) methods are used for further thermodynamic correlations. B3LYP-D3 and MP2 values were extrapolated toward the CBS.[31] CCSD(T)/CBS values were estimated from MP2/CBS values, and the difference between CCSD(T) and MP2 energies was evaluated with the aug-cc-pVDZ basis set.[42] B3LYP-D3 data were calculated in software package Molpro 2012.1,[43] and MP2 and CCSD(T) data were calculated in Gaussian 03 (G03).[44]

2.2. Phonon Properties. Electronic structure and phonon properties of the crystalline phases were calculated in our previous work[38] using the PAW formalism[45] and the optPBE-vdW functional[46] as implemented in the program package VASP.[47] A plane wave energy cutoff of 1000 eV was used for the periodic DFT calculations, along with the so-called hard PAW potentials and the Monkhorst−Pack sampling of the k-space.[48] All the crystal structures were optimized, keeping only their space group of symmetry constrained. After that, the electronic energy of the unit cell $[E^{\text{cr}}_{\text{el}}(V)]$ was calculated as a function of its volume by assuming the isotropic expansive behavior of the crystals. Phonon properties were calculated for supercells (larger than 10 Å in all directions) created by replication of the optimized unit cells using a finite displacement method[49] and the program Phonopy.[50] In this way, the density of phonon states was calculated for five unit cell volumes, which enabled the construction of the vibrational Helmholtz energy $[A^{\text{cr}}_{\text{vib}}(T,V)]$ as a function of both temperature and volume, as needed by the quasi-harmonic approximation.[34] Summation of $E^{\text{cr}}_{\text{el}}(V)$ with $A^{\text{cr}}_{\text{vib}}(T,V)$ yielded total Helmholtz energy profiles $[A^{\text{cr}}_{\text{tot}}(T,V)]$ of the unit cell, which were subsequently, for each temperature separately, fitted by the Murnaghan equation of state,[51] providing volume-dependent Helmholtz energy profiles at finite temperatures in an analytical form. On the basis of these, the thermodynamic properties, such as Gibbs energy $[G^{\text{cr}}_{\text{tot}}(T,p)]$ and isobaric heat capacity $[C^{\text{cr}}_{p}(T,p)]$, could be evaluated using fundamental thermodynamic relations.

2.3. Vapor Phase. The vapor phase was treated as an ideal gas, the isobaric heat capacity ($C^{\text{g},0}_{p}$) of which was calculated using the rigid rotor−harmonic oscillator (RRHO) model.[35] Optimizations of molecular structures and computations of molecular fundamental vibration frequencies and eventually of their barriers to internal rotation motions were carried out with Gaussian 03,[44] using the B3-LYP functional[40,41] and the split-valence basis set 6-311+G(d,p). The calculated frequencies were scaled by the empirical factors developed in our previous works to minimize the uncertainty in calculated $C^{\text{g},0}_{p}$.[52] For more flexible molecules in which internal rotations take place, the one-dimensional hindered rotor (1D-HR) scheme was employed to account for respective corrections to $C^{\text{g},0}_{p}$,[36] using the calculated barriers to internal rotations and the reduced moments of inertia evaluated according to formulas developed by Pitzer et al.[53,54] Solutions of appropriate one-dimensional Schrödinger equations were obtained using our code following the FGH method.[55] The existence of several conformers and their equilibrium in the vapor phase in the case of flexible molecules[56] (e.g., butane) were neglected since the temperatures of interest in this work are very low and only the most stable conformer dominates under such conditions.

At the classical high-temperature limit, both translation and rotation terms contribute a value of 3/2 R to $C^{\text{g},0}_{p}$ (rotation of only R in the case of linear molecules). At very low temperatures, however, the higher rotational energy levels may not be populated sufficiently, and the partition function of the rotation motion has to be evaluated explicitly by summation over the first N energy levels until its convergence is reached.[37] Such treatment becomes necessary in the region of temperatures around or below the rotation temperature defined as

$$\Theta^{\text{Rot}}_{\text{i}} = \frac{\hbar^2}{2k_{\text{B}}I_{\text{i}}} \tag{2}$$

where $\hbar$ and k_{B} are the reduced Planck and Boltzmann constants, respectively, and I_{i} denotes one of the principal molecular moments of inertia. Obviously, it holds that the smaller the molecule is, the higher the rotation temperatures that should be expected (for hydrogen molecule being an extreme case, the rotation partition function needs to be summated explicitly even at 100 K). Using this explicit summation over the rotation levels in the vicinity of 0 K, one obtains that the rotation contribution to $C^{\text{g},0}_{p}$ steeply increases up to a maximum point and only then gradually converges to the respective 3/2 R or R high-temperature limits, depending on molecular linearity. For small molecules, this phenomenon occurs typically in the region below 30 K. Among the studied molecules in our test set, hydrogen fluoride exhibits the highest $\Theta^{\text{Rot}}_{\text{i}} = 29.3$ K.

Another quantum effect that should be taken into account for symmetric molecules is that the population of their rotation energy levels is related to the nuclear spin, which is generally coupled with the rotation partition function while the total wave function has to be either symmetric or asymmetric to interchanges of particles (atomic nuclei with integer or half-integer spin, respectively) represented by certain rotations of a given molecule. As a result, particular rotation levels possess different degeneracies and need to be counted with appropriate weights in the rotation partition function. Again, this effect occurs most significantly for the lightest molecule, hydrogen. Weights of particular rotation levels can be determined by general group theory considerations, summarized by McQuarrie[37] for diatomic molecules and pioneered by Wilson[57] for more complex molecules possessing at least a 2-fold rotation axis.

In the vicinity of absolute zero, the rotation partition functions were evaluated by direct summation over the lowest 500 energy levels for all 22 molecules until the rotation term

DOI: 10.1021/acs.jctc.7b00164
J. Chem. Theory Comput. 2017, 13, 2840−2850

became constant (3/2 R or R, depending on molecular linearity) with increasing temperature. In the case of molecules not possessing at least a 3-fold axis of symmetry, an approximation had to be accepted. Such small molecules, typically having C_2 symmetry, possess three different moments of inertia, which hinder the explicit evaluation of the rotation energy levels. However, two of these moments of inertia usually lie very close to each other so that their average values were considered along with the third different value of the moment of inertia. Such a simplification enables one to calculate the rotation partition function for the whole test set of molecules analytically while the underlying uncertainty in $C_p^{g,0}$ is expected to be negligible, given the narrow temperature interval over which this issue is relevant. Nuclear spin conversion effects were assumed for ethyne, nitrogen, fluorine, carbon dioxide, ammonia, and formaldehyde.

As long as the translation energy levels are much denser on the energetic scale than the rotational levels, their discrete character and corresponding quantum effects take place at much lower temperatures than in the case of the rotation motion. According to Irikura et al.,[35] the translation term can be evaluated classically when the criterion

$$T^{5/2}p^{-1} >> (2\pi)^{-3/2}h^3k_B^{-5/2}m^{-3/2} \quad (3)$$

is met, where h stands for the Planck constant and m represents the molecular mass, T the temperature, and p the pressure. For methane, for example, both sides of eq 3 are comparable at around 0.01 K. Above this temperature, the translation term can be regarded as a constant 3/2R. Taking into account that this issue is relevant only in an extremely narrow temperature range, integration of $C_p^{g,0}$ is expected to cause enthalpic uncertainties amounting to fragments of a kJ·mol^{-1}.

2.4. Minor Contributions to Sublimation Enthalpy. Provided that the optimized molecular geometries were obtained for both the vapor and crystal phases, the geometry relaxation term $\Delta_{geom}^{cr\rightarrow g}E$ was evaluated as the difference of energies of (i) a molecule from the crystal lattice optimized using optPBE-vdW functional[46] in VASP (crystal phase), which was further assumed as an isolated molecule the energy of which was recalculated with the PBE functional[58] in G03 without further optimization, and (ii) an isolated molecule fully optimized using the PBE functional in G03.

$\Delta_{ZPE}^{cr\rightarrow g}E$ terms were calculated as the difference of (i) the ZPVE of the crystals, based on the optPBE-vdw phonon calculations using the Γ-point vibrational frequencies υ_i and the harmonic approximation formula 1/2 $h\upsilon_i$, and (ii) the ZPVE from the vibrational frequencies of an isolated molecule optimized using the PBE functional and the harmonic approximation.

$H_{therm}^{lattice}$ and $H_{ro\text{-}tr}^{g}$ terms were implicitly included in the calculated thermal enthalpies of both phases calculated using essential statistical thermodynamic relations.

2.5. Reference Experimental Data. Critically assessed experimental data, used in this work as a benchmark set for validation of the computational methodology, were developed by multiproperty thermodynamic correlations in our previous work,[17] which provides details on this procedure and the estimation of uncertainties of reference experimental data as well as a list of primary sources of experimental thermodynamic data (see Table 3 in ref 17). Temperature-dependent $\Delta_{sub}^{exp}H$ values were obtained by a temperature adjustment of $\Delta_{sub}^{exp}H$ known at a given temperature and corresponding experimental C_p^{cr} and calculated $C_p^{g,0}$ values, summarized by the equation

$$\Delta_{sub}H(T) = \Delta_{sub}H(T_0) + \int_{T_0}^{T} [C_p^{g,0}(T') - C_p^{cr}(T')]\,dT' \quad (4)$$

3. RESULTS AND DISCUSSION

In this section, all the contributing terms to $\Delta_{sub}H$, as given in eq 1, are discussed and their uncertainties analyzed. It is legitimate to assume that the cohesive energy E_{coh} represents the dominant contribution to $\Delta_{sub}H$. Furthermore, at least the $H_{therm}^{lattice}$ and $H_{ro\text{-}tr}^{g}$ terms unconditionally need to be included to obtain qualitatively reasonable behavior of $\Delta_{sub}H$, while the remaining terms usually play a rather minor role and are thus often neglected in some simpler computational schemes.

3.1. Vapor Phase at Very Low Temperatures. Taking into account the results of the previous studies on the reliability of the calculations of the thermodynamic properties,[36,52,59−61] we conservatively estimate the uncertainty of our calculated $C_p^{g,0}$ to be below 2% at higher temperatures (above 100 K in this case). The situation in the vicinity of 0 K deserves, however, some attention as long as the rotational contribution $C_{rot}^{g,0}$ cannot be considered as a constant close to the absolute zero. Figure 1 represents an example of calculated $C_{rot}^{g,0}$ terms for

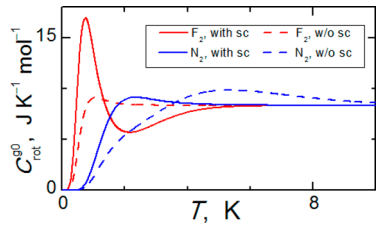

Figure 1. Illustration of the nuclear spin conversion effects on the rotational contributions to $C_p^{g,0}$ of molecular fluorine and nitrogen at very low temperatures.

molecular nitrogen and fluorine using a direct summation of the rotation partition function over the lowest 500 energy levels. Neglecting the spin effects leads to similar curves for both gases. $C_{rot}^{g,0}$ steeply increases toward a maximum and then slowly converges to the constant value of R, and only the maximum for the lighter molecule of nitrogen is shifted to higher temperature. Taking the nuclear spin effects into account, a difference in the shape of $C_{rot}^{g,0}$ curves for the two gases occurs as long as the rotation energy levels of a N_2 molecule, containing dominantly the isotope ^{14}N having integer spin +1 so that such nuclei are bosons, exhibit different multiplicity compared to a F_2 molecule, containing ^{19}F nuclei possessing a half-integer spin +1/2, thus fermions. The $C_{rot}^{g,0}$ curve for the F_2 molecule, being a heavier analogue of H_2, exhibits an even more significant maximum which is followed by a minimum and only then the constant R level is reached. Such a curve for N_2 does not exhibit any minimum, and the nuclear spin effects only shift the maximum of $C_{rot}^{g,0}$ toward higher temperature and make it flatter. Nevertheless, such a behavior of $C_{rot}^{g,0}$ affects the values of integral quantities like $\Delta_{sub}H$ only at temperatures below 30 K, and still, its influence is very small compared to the cohesive energies amounting to tens of kJ·mol^{-1}. Moreover, values of the integral $\int C_{rot}^{g,0}(T)\,dT$ obtained by both models differ by no more than 1 J·mol^{-1} when integrating over a broad temperature range. To illustrate the temperature range where $C_{rot}^{g,0}$ should not be taken as constant, relevant rotational temperatures calculated for the

DOI: 10.1021/acs.jctc.7b00164
J. Chem. Theory Comput. 2017, 13, 2840−2850

Table 1. Calculated Cohesive Energies E_{coh}^{cr} (kJ mol^{-1}), Individual Contributions to Sublimation Enthalpy $\Delta_{sub}^{calc}H$ Evaluated at T = 0 K, and Comparison with Experimental Reference Values $\Delta_{sub}^{exp}H(0K)$

molecule	E_{coh}^{cr} [a]	$\Delta_{geom}^{cr\rightarrow g}E$ [b]	$\Delta_{ZPE}^{cr\rightarrow g}E$ [c]	$\Delta_{sub}^{calc}H(0K)$ [d]	$\Delta_{sub}^{exp}H(0K)$ [e]
neon	−2.10	0.00	−1.23	0.87	1.9 ± 0.2
argon	−8.00	0.00	−0.98	7.02	7.8 ± 0.2
ethane	−22.64	−0.01	−3.38	19.25	20.3 ± 0.5
ethene	−17.30	−0.02	−3.82	13.46	19.0 ± 0.5
ethyne	−27.03	−0.20	−3.28	23.55	
propane	−23.57	−0.27	−3.33	19.97	27.5 ± 0.5
butane	−37.37	−0.26	−3.68	33.43	34.0 ± 0.4
nitrogen	−8.45	−0.07	−1.76	6.62	6.9 ± 0.1
fluorine	−9.55	−0.55	−2.34	6.66	8.2 ± 0.3
carbon dioxide	−21.15	−0.13	−2.24	18.78	26.3 ± 0.3
ammonia	−39.13	−0.35	−8.69	30.09	29.5 ± 0.6
hydrogen peroxide	−73.31	−8.04	−7.59	57.68	59.8 ± 2.0
hydrogen fluoride	−42.37	−5.43	−7.75	29.19	29.3[f]
methanol	−53.78	−2.58	−6.62	44.58	45.7 ± 0.3
formaldehyde	−35.27	−2.07	−8.85	24.35	
aminomethane	−36.31	−0.06	−6.14	30.11	36.9 ± 0.8
dimethyl ether	−30.23	−0.74	−4.51	24.98	31.9 ± 0.6
hydrazine	−51.22	−2.38	−8.02	40.82	58.3 ± 1.0
methylhydrazine	−50.41	−6.21	−6.33	37.87	55.9 ± 1.0
formic acid	−53.33	−9.97	−4.92	38.44	60.4 ± 1.0
formamide	−89.85	−6.97	−7.94	74.94	72.9 ± 0.7
acetic acid	−70.64	−8.08	−4.46	58.10	67.0 ± 2.0

[a]Cohesive energies calculated at the CCSD(T)/CBS level using a fragment-based additive scheme taken from our previous work.[17] [b]Energy change related to the relaxation of a molecule from its geometry in the crystalline phase to the geometry of an isolated molecule in the vapor phase. Values were calculated using the PBE functional within the DFT formalism. [c]Difference in the zero-point vibrational energies of the vapor and crystal phases based on optPBE-vdw phonon calculations for the crystal phases and PBE calculations of the harmonic fundamental vibrational modes for isolated molecules. [d]Calculated sublimation enthalpy at T = 0 K. [e]Experimental sublimation enthalpies adjusted to T = 0 K. Blank spaces mean that it was not possible to reliably extrapolate $\Delta_{sub}^{exp}H$ down to 0 K due to the lack of experimental data on C_p^{cr}. [f]Experimental value cannot be determined precisely due to molecular association in the vapor phase, which has not been fully explained in the literature.

studied molecules are summarized in the Supporting Information in Table S1.

3.2. Sublimation Enthalpy. Since E_{coh}^{cr} is the dominant contribution to $\Delta_{sub}H$, it is crucial to perform its calculation at the highest possible level of theory. Various aspects of ab initio calculations of E_{coh}^{cr} have been discussed in several recent literature works,[16,17,20,29,62] so we will repeat only the most important points here. In this work, we compare final $\Delta_{sub}H$ values calculated using the fragment-based additive scheme and three quantum chemistry methods, namely, B3LYP-D3/CBS, MP2/CBS, and CCSD(T)/CBS. The vibration-based and thermal contributions to enthalpy play a rather minor role for the overall accuracy of calculated $\Delta_{sub}H$, so less expensive DFT calculations of vibrational degrees of freedom are accepted as sufficient for both phases.

Table 1 summarizes all the terms required to evaluate $\Delta_{sub}H$ at 0 K, namely, CCSD(T)/CBS-based E_{coh}^{cr}, DFT-based $\Delta_{geom}^{cr\rightarrow g}E$, and $\Delta_{ZPE}^{cr\rightarrow g}E$ terms, along with calculated $\Delta_{sub}^{calc}H$ and experimental $\Delta_{sub}^{exp}H$ values at 0 K. The $\Delta_{geom}^{cr\rightarrow g}E$ terms are always negative (except for monatomic gases neon and argon) since the molecules can take their most advantageous geometries in the vapor phase without any constraints caused by the presence of other molecules in the crystal lattice. A typical example is the formation of the hydrogen bonds in the crystal, which leads to conformations distorted from the optimized vapor-phase molecular structures. This phenomenon occurs to a higher extent for hydrogen peroxide, for which the outstanding value of $\Delta_{geom}^{cr\rightarrow g}E$ arises since the trans conformation is conserved in the crystal to maximize the energy gain from the formation of hydrogen bonds, while isolated H_2O_2 molecules are predicted to exhibit a gauche conformation.

In principle, the sign of the $\Delta_{ZPE}^{cr\rightarrow g}E$ terms is not predetermined as in the previous case. However, it is much more probable that $\Delta_{ZPE}^{cr\rightarrow g}E$ is negative, as evidenced by our 22-molecule set, for all of which $\Delta_{ZPE}^{cr\rightarrow g}E$ is negative. This is caused by the lattice vibrational modes which are absent in the gaseous phase, so ZPVE of the crystal phase is higher while the intramolecular modes usually do not differ to an extent that would override this trend. The $\Delta_{ZPE}^{cr\rightarrow g}E$ term is more significant for polar molecules, for which crystals exhibit higher lattice mode frequencies due to stronger intermolecular interactions. The highest $\Delta_{ZPE}^{cr\rightarrow g}E$ values among the studied compounds were observed for hydrogen peroxide and ammonia, which both reach almost 10 kJ mol^{-1}.

Including the $\Delta_{geom}^{cr\rightarrow g}E$ and $\Delta_{ZPE}^{cr\rightarrow g}E$ terms into the evaluation of $\Delta_{sub}^{calc}H$ brings $\Delta_{sub}^{calc}H$ to a very good agreement with $\Delta_{sub}^{exp}H$ for some hydrogen-bonded crystals, e.g., hydrogen peroxide or hydrogen fluoride, the calculated E_{coh}^{cr} values of which were largely higher in absolute value than the final $\Delta_{sub}^{calc}H$. On the other hand, including $\Delta_{geom}^{cr\rightarrow g}E$ and $\Delta_{ZPE}^{cr\rightarrow g}E$ led to the significant underestimation of $\Delta_{sub}^{calc}H$ for hydrazine and methylhydrazine. On the basis of particular values in Table 1, it seems reasonable to expect that especially $\Delta_{geom}^{cr\rightarrow g}E$ is often overestimated in absolute value, which can eventually compensate for the overestimated E_{coh}^{cr} values. It is, however, more likely that E_{coh}^{cr} would be underestimated,[17] leading together with too negative values of $\Delta_{geom}^{cr\rightarrow g}E$ and $\Delta_{ZPE}^{cr\rightarrow g}E$ to larger underestimations of the final $\Delta_{sub}^{calc}H$. Calculated $\Delta_{sub}^{calc}H$ could not be directly compared to their experimental counterparts $\Delta_{sub}^{exp}H$ for the whole test set,

DOI: 10.1021/acs.jctc.7b00164
J. Chem. Theory Comput. 2017, 13, 2840−2850

since the experimental data for C_p^{cr} needed to adjust $\Delta_{sub}^{exp}H$ were not always available at temperatures close enough to 0 K, as indicated in Table 1 for ethyne and formaldehyde.

Adding the thermal contributions to the enthalpies of both phases ($\Delta_{therm}^{cr\rightarrow g}E$, $-H_{therm}^{lattice}$, and $H_{ro\text{-}tr}^{g}$ in eq 1) leads to the temperature-dependent $\Delta_{sub}H$. Its temperature adjustment from 0 K can be done according to eq 4, where T_0 = 0 K.

Examples of calculated $\Delta_{sub}H(T)$ curves for ethane, butane, ammonia, and methanol are given in Figure 2. $\Delta_{sub}H(T)$ values

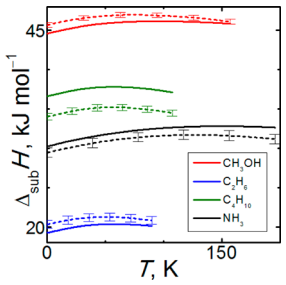

Figure 2. Examples of temperature trends of $\Delta_{sub}^{calc}H$ (solid lines) and $\Delta_{sub}^{exp}H$ (dashed lines) along with their expanded uncertainties for methanol, butane, ammonia, and ethane.

for these compounds steadily increase with rising temperature from 0 K until a maximum is reached at a temperature $T(\Delta_{sub}^{max}H)$, and yet then the expected decrease can be seen. At first sight, such obtained nonmonotonous behavior of $\Delta_{sub}H$ seems to be against a common chemical engineering sense, especially the fact that $\Delta_{sub}H(T)$ increases with temperature under certain conditions, even though such a behavior has recently been reported for water ice,[63] carbon dioxide,[32,64] and α,ω-diamines.[56] The mathematical explanation of this behavior is illustrated in Figure 3 and is based on the determination of

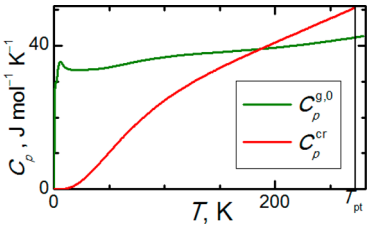

Figure 3. Temperature trends of calculated $C_p^{g,0}$ and C_p^{cr} for hydrogen peroxide.

the sign of the $C_p^{g,0}(T) - C_p^{cr}(T)$ difference at a given temperature. Analyzing the common trends and magnitudes of $C_p^{g,0}$ and C_p^{cr}, it can be seen that C_p^{cr} scales as T^3 at very low temperatures and its increase becomes less steep as the temperature increases, while $C_p^{g,0}$ reaches its constant sum of translational and rotational contributions $4R$ (for nonlinear molecules) very quickly and starts slowly increasing further only after the intramolecular vibrations become thermally excited. This means that $C_p^{g,0} > C_p^{cr}$ at a certain interval of low temperatures. $\Delta_{sub}H$ naturally reaches its maximum at $T(H_{sub}^{max})$ when $C_p^{g,0} = C_p^{cr}$ holds.

Table 2 lists the maximum values of $\Delta_{sub}^{exp}H$ and corresponding temperatures $T(\Delta_{sub}^{max}H)$ determined by a temperature adjustment of experimental data for $\Delta_{sub}^{exp}H$, performed according to eq 4 (see Table 3 in ref 17 for the list of original experimental works) for all 22 studied crystals, except for only ethyne and formaldehyde, for which calculated C_p^{cr} was used due to the lack of experimental C_p^{cr} data. For several compounds, the phase transition point is reached before the maximum of $\Delta_{sub}^{calc}H$ (i.e., neon, nitrogen, and fluorine), so in such cases, $\Delta_{sub}^{calc}H$ would exhibit its maximum at the temperature of the lowest-lying phase transition (T_{pt}). However, such behavior was not observed for $\Delta_{sub}^{exp}H$. Another validation statistics of the uncertainty of calculated C_p^{cr} data from ref 38 is given in Table 2, which compares the temperatures $T(\Delta_{sub}^{max}H)$, determined either using calculated or experimental data for C_p^{cr}. On average, the fully calculated $T(\Delta_{sub}^{max}H)$ values are overestimated by 18% when compared to their experimental counterparts, which points to a prevailing underestimation of given calculated C_p^{cr} data. The smallest deviations of calculated $T(\Delta_{sub}^{max}H)$ do not exceed 1.0 K (for carbon dioxide or hydrogen fluoride), while the largest deviation of 22 K occurs for ammonia.

Next, Table 2 summarizes the comparison of calculated and experimental $\Delta_{sub}H$ evaluated at T_{pt} for all 22 studied crystals. Concerning the agreement of $\Delta_{sub}^{calc}H$ and $\Delta_{sub}^{exp}H$ at T_{pt}, there are species for which a very good agreement was reached, e.g., argon, ethane, or methanol. In these cases, the two values do not differ by more than 1 kJ mol^{-1}, which is comparable to the uncertainty of the experimental determinations. On the other hand, there are examples of unexpected failures of the computational model, as for ethene or formaldehyde, where $\Delta_{sub}^{calc}H$ differs from $\Delta_{sub}^{exp}H$ by more than 5 kJ mol^{-1}, or even 10 kJ mol^{-1} for hydrazine. In general, there are crystals (carbon dioxide or hydrazine) in the testing set for which the periodic-DFT-based C_p^{cr} values exhibit high accuracy, but their FBAS cohesive energies do not correspond to the experimental values of sublimation enthalpies. Also, several examples can be found where the situation is the opposite (neon or nitrogen), whereas both types of calculations exhibit high accuracy, for example, for butane or ammonia. This happens because both parts of the computational methodology (FBAS lattice energies and periodic-DFT-based phonon properties) use completely different quantum levels of theory, which may succeed or fail in different situations.

To display the temperature-dependent deviations of $\Delta_{sub}^{calc}H$ from $\Delta_{sub}^{exp}H$, a percentage deviation quantity

$$\sigma_H(T) = \frac{\Delta_{sub}^{calc}H(T) - \Delta_{sub}^{exp}H(T)}{\Delta_{sub}^{exp}H(T)} \quad (5)$$

was defined. A plot of $\sigma_H(T)$ trends for the studied crystals is given in Figure 4 using a reduced temperature ($T_r = T/T_{pt}$) coordinate for the x axis to deal with the different widths of temperature stability intervals for individual crystals. Averaging $|\sigma_H|$ over the whole studied crystal set yields a 15% value at 0 K and 12% at T_r = 1, meaning that a closer agreement of theory and experiment has been reached for the higher temperatures. As long as the quasi-harmonic approximation is expected to fail to account for large anharmonic effects at higher temperatures, such a trend in $\sigma_H(T)$ points rather to a fortuitous compensation of errors of FBAS lattice energies and periodic-DFT-based phonon calculations.

Clearly, the main source of the computational uncertainty remains in the calculation of the cohesive energy, the eventual underestimation of which by the FBAS cannot be later corrected by the periodic-DFT-based thermal contributions. Another considerable uncertainty term is represented by the $\Delta_{ZPE}^{cr\rightarrow g}E$ term, since it is based on the phonon frequencies exhibiting a significant scatter. Too negative values of the

DOI: 10.1021/acs.jctc.7b00164
J. Chem. Theory Comput. 2017, 13, 2840−2850

Table 2. Calculated and Experimental Sublimation Enthalpies $\Delta_{sub}H$ (kJ mol^{-1}) at the Temperatures of Lowest-Lying Phase Transitions (T_{pt}, in K) along with the Maxima of $\Delta_{sub}H$ for the Low-Temperature Polymorphs

molecule	$T^{calc}(\Delta_{sub}^{max}H)$[a]	$T^{exp}(\Delta_{sub}^{max}H)$[b]	$\Delta_{sub}^{max}H$[c]	T_{pt}[d]	$\Delta_{sub}^{calc}H(T_{pt})$	$\Delta_{sub}^{exp}H(T_{pt})$[e]
neon	41.02	24.57	2.2	24.69	1.30	2.2 ± 0.2
argon	50.30	34.84	8.2	80.81	7.46	7.9 ± 0.2
ethane	57.04	51.32	21.3	89.81	20.12	20.8 ± 0.5
ethene	62.52	53.38	20.0	103.97	14.29	19.3 ± 0.5
ethyne	72.43		24.7[f]	142.70	24.18	24.5 ± 1.0
propane	52.79	51.26	28.6	85.33	20.68	28.2 ± 0.5
butane	56.96	55.96	35.2	107.55	33.91	34.5 ± 0.4
nitrogen	39.41	26.57	7.3	35.61	7.23	7.3 ± 0.1
fluorine	48.85	33.43	8.8	45.55	7.53	8.8 ± 0.3
carbon dioxide	58.50	57.82	27.3	216.59	17.32	24.9 ± 0.3
ammonia	149.97	127.34	31.7	195.48	32.46	31.2 ± 0.6
hydrogen peroxide	186.68	171.43	62.5	272.74	60.14	61.8 ± 2.0
hydrogen fluoride	166.50	167.45	31.4	189.79	31.41	31.4[g]
methanol	96.19	73.89	47.0	157.34	45.81	46.1 ± 0.3
formaldehyde	121.25[e]		26.5[f]	155.17	26.31	34.2 ± 1.5
aminomethane	88.63	77.61	38.3	101.52	31.61	38.2 ± 0.8
dimethyl ether	62.73	56.23	32.9	131.66	25.48	32.0 ± 0.6
hydrazine	128.05	124.8	60.4	274.69	41.21	58.8 ± 1.0
methylhydrazine	92.07	86.1	57.4	220.79	38.44	56.2 ± 1.0
formic acid	102.03	94.1	61.9	281.40	38.49	59.8 ± 1.0
formamide	111.29	97.8	74.2	275.54	75.29	72.1 ± 0.7
acetic acid	75.67	69.3	68.3	289.69	55.50	65.2 ± 2.0

[a]Calculated temperature at which $\Delta_{sub}^{exp}H$ reaches its maximum on the temperature interval (0, T_{pt}). [b]Experimentally determined temperature at which $\Delta_{sub}^{exp}H$ reaches its maximum on the temperature interval (0, T_{pt}). [c]Maximum value of $\Delta_{sub}^{exp}H$ determined by a temperature adjustment of experimental data (see eq 4) for C_p^{cr}, $\Delta_{sub}^{exp}H$, and calculated $C_p^{g,0}$. [d]Temperature of the first phase transition, either solid−solid or solid−liquid. [e]Estimated experimental expanded uncertainty (coverage factor $k = 2$) is considered to be rather constant with temperature. [f]Calculated value had to be used due to the lack of experimental data required for the correlation. [g]Experimental value cannot be determined precisely due to molecular association in the vapor phase, which has not been fully explained in the literature.

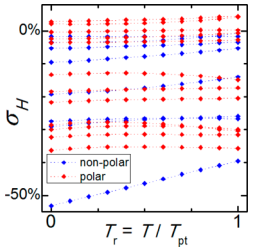

Figure 4. Temperature trends of relative percentage deviations σ_H (eq 5) of $\Delta_{sub}^{calc}H$, evaluated using E_{coh}^{cr} calculated at the CCSD(T)/CBS level of theory, from $\Delta_{sub}^{exp}H$.

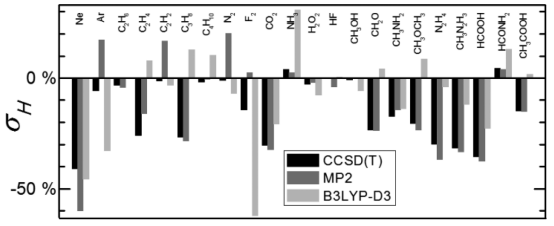

Figure 5. Comparison of $\Delta_{sub}^{calc}H$ at T_{pt} evaluated using E_{coh}^{cr} calculated at the CCSD(T)/CBS, MP2/CBS, and B3LYP-D3/CBS levels of theory with $\Delta_{sub}^{exp}H$ (for the definition of σ_H, see eq 5).

$\Delta_{ZPE}^{cr\rightarrow g}E$ and $\Delta_{geom}^{cr\rightarrow g}E$ terms, together with often underestimated E_{coh}^{cr}, are the main reasons for inaccurate (too low) values of $\Delta_{sub}^{calc}H$ which were underestimated in 78% of cases from the testing set. Using the empiric scale factors, a common practice to lower the uncertainty related to calculated vibrational frequencies, is of no use in this case because it is hardly possible to develop reliable scale factors for the lattice modes due to the lack of experimental data. Moreover, scaling the frequencies of both phases by different factors seems to be a major inconsistency. Therefore, we prefer not to scale the calculated vibrational frequencies for evaluations of $\Delta_{ZPE}^{cr\rightarrow g}E$ at this point. The uncertainty arising from the calculated thermal contributions is expected to be 1 or 2 orders of magnitude lower than that of E_{coh}^{cr}.

Figure 5 summarizes the comparison of $\Delta_{sub}^{calc}H$ evaluated using three various quantum chemical methods for calculation of E_{coh}^{cr}, but the same phonon-based terms: CCSD(T)/CBS-based $\Delta_{sub}^{CCSD(T)}H$, MP2-based $\Delta_{sub}^{MP2}H$, and B3LYP-D3/CBS-based $\Delta_{sub}^{D3}H$. On average, $\Delta_{sub}^{CCSD(T)}H$ and $\Delta_{sub}^{D3}H$ exhibit a mean absolute percentage deviation from experimental data equal to 15%, while $\Delta_{sub}^{CCSD(T)}H$ lies closer to $\Delta_{sub}^{exp}H$ than $\Delta_{sub}^{D3}H$ in exactly half of the studied cases. It holds that $\Delta_{sub}^{D3}H > \Delta_{sub}^{CCSD(T)}H$ in 68% of cases. The same mean absolute percentage deviation amounts to 18% for $\Delta_{sub}^{MP2}H$, while $\Delta_{sub}^{CCSD(T)}H$ is more accurate in 64% of cases. When $\Delta_{sub}^{CCSD(T)}H$ and $\Delta_{sub}^{D3}H$ are compared for the individual crystals, $\Delta_{sub}^{D3}H$ typically fails to reproduce the experimental counterparts for weakly dispersion bound crystals of rare gases. The same trend was also observed for ethyne or butane for which $\Delta_{sub}^{CCSD(T)}H$ is in very good agreement with the experiment. On the other hand, $\Delta_{sub}^{D3}H$ is more successful in reproducing the experimental data for hydrogen-bound crystals, such as formic acid, acetic acid, hydrazine, or methylhydrazine, for which $\Delta_{sub}^{CCSD(T)}H$ is unexpectedly strongly underestimated. We assume that this happens mostly due to too negative $\Delta_{geom}^{cr\rightarrow g}E$ terms. To break this trend, an opposite situation was observed for formamide.

DOI: 10.1021/acs.jctc.7b00164
J. Chem. Theory Comput. 2017, 13, 2840−2850

Particular $\Delta_{sub}^{calc}H$ values for all studied crystals are summarized in the Supporting Information (Table S2). Usually, CCSD(T)/CBS results for E_{coh}^{cr} are lower in absolute value than their MP2 or DFT-D3 analogues. Therefore, in conjunction with with too negative $\Delta_{ZPE}^{cr\rightarrow g}E$ and $\Delta_{geom}^{cr\rightarrow g}E$ terms, DFT-D3-based E_{coh}^{cr} can in some cases yield $\Delta_{sub}^{calc}H$ lying in a closer agreement with experiment than the CCSD(T)-based E_{coh}^{cr} due to a fortuitous compensation of errors.

To further illustrate the importance of the accuracy of calculations of E_{coh}^{cr}, we used the recently published literature values on E_{coh}^{cr} (and optionally $\Delta_{geom}^{cr\rightarrow g}E$), culled from Table 4 in ref 17 and calculated using various levels of theory, coupled with the vibrational and thermal terms calculated in this work, to evaluate $\Delta_{sub}^{calc}H$ and show its resulting scatter, as given in Table 3 for a subset of 12 crystals. On the basis of this analysis,

Table 3. Illustration of the Scatter of $\Delta_{sub}^{calc}H$ (kJ·mol^{-1}) Calculated at 0 K Using Various Literature Values of E_{coh}^{cr} and $\Delta_{sub}^{calc}H$ Values in the Closest Agreement with $\Delta_{sub}^{exp}H$

molecule	$\Delta_{sub}^{lowest}H$[a]	$\Delta_{sub}^{highest}H$[a]	$\Delta_{sub}^{best}H$[b]	$\Delta_{sub}^{exp}H$[c]
neon	0.1[69]	4.4[26]	2.0[68]	1.9 ± 0.2
argon	6.5[23]	7.7[68]	7.7[68]	7.8 ± 0.2
ethyne[d]	23.1[71]	29.9[65]	24.2[17,71]	24.5 ± 1.0
propane	20.0[17]	31.1[73]	24.4[73]	27.5 ± 0.5
nitrogen	6.6[17]	7.6[65]	6.6[17]	6.9 ± 0.1
carbon dioxide	18.8[17]	32.2[69]	26.2[75,76]	26.3 ± 0.3
ammonia	17.5[71]	39.0[73]	29.8[62]	29.5 ± 0.6
hydrogen fluoride[e]	29.2[17]	31.2[80]	29.2[17]	29.3
methanol	44.6[17]	56.2[81]	44.6[17]	45.7 ± 0.3
formic acid	38.4[17]	63.8[73]	59.0[71]	60.4 ± 1.0
formamide	60.5[78]	78.9[29]	72.8[77]	72.9 ± 0.7
acetic acid	58.1[17]	79.2[29]	67.3[29]	67.0 ± 2.0

[a] $\Delta_{sub}^{calc}H$ calculated using the extreme literature values of $|E_{coh}^{cr}|$, culled from literature to our best knowledge, coupled with the vibrational and thermal terms calculated in this work along with the reference to the original calculations of $|E_{coh}^{cr}|$. [b] $\Delta_{sub}^{calc}H$ calculated using the literature values of $|E_{coh}^{cr}|$ and optionally $\Delta_{geom}^{cr\rightarrow g}E$, coupled with the vibrational and thermal terms calculated in this work, being in the closest agreement to $\Delta_{sub}^{exp}H$ along with the reference to the original calculations of $|E_{coh}^{cr}|$. [c] Experimental sublimation enthalpies adjusted to T = 0 K. [d] Values corresponding to the transition point temperature 142.7 K had to be used due to the lack of experimental data at low temperatures. [e] Experimental value and its uncertainty cannot be determined precisely due to molecular association in the vapor phase, which has not been fully explained in the literature.

the relative scatter of the extreme values of $\Delta_{sub}^{calc}H$ exceeds 100% for many of the selected crystals, while the differences of $\Delta_{sub}^{calc}H$ obtained using various E_{coh}^{cr} values range in units or tens of kJ·mol^{-1}.

As it was estimated in our previous work,[17] the cohesive energies used in this work for the evaluation of $\Delta_{sub}^{calc}H$ can be burdened by an uncertainty amounting to 10−20%, caused mainly by a finite cutoff for the dispersion interactions, too crude nonpolarizable point-charge-based long-range electrostatic model, or not sufficiently converged three-body interaction sums. In some cases, our FBAS calculations[17] yielded significantly underbound crystals resulting in lower E_{coh}^{cr} in absolute values, which lead to higher $|\sigma_H|$ values. To eliminate this issue and to study it more closely, we searched for the literature values of E_{coh}^{cr} to use them, along with the remaining terms in eq 1 calculated in this work, to evaluate $\Delta_{sub}^{calc}H$. In this way, we were able to compare and rank the performance of various popular quantum chemical methods. If possible, this analysis was performed at 0 K to minimize the noise effects of all thermal contributions. All $\Delta_{sub}^{calc}H$ calculated using particular literature values on E_{coh}^{cr} are summarized in the Supporting Information (Table S3) along with an assessment of the accuracy of such values. To our best knowledge, calculated E_{coh}^{cr} values from the literature were found for crystals of neon,[26,62,65−69] argon,[23,26,62,65,66,68−70] ethyne,[23,65,71] propane,[72,73] nitrogen,[65] carbon dioxide,[23−25,27−29,62,71,73−78] ammonia,[24,27−29,62,69,71,73−78] hydrogen fluoride,[79,80] methanol,[81] formic acid,[71,73] formamide,[24,27−29,62,72−74,77,78] and acetic acid.[27,29,62,74,77] If our FBAS-based E_{coh}^{cr} values were substituted for other relevant calculated data from the literature for E_{coh}^{cr}, $|\sigma_H|$ values close to zero would be obtained for some of the mentioned crystals, e.g., carbon dioxide, formic acid, or acetic acid. On the other hand, our FBAS-based E_{coh}^{cr} values resulted in $\Delta_{sub}^{calc}H$ being in the best agreement with $\Delta_{sub}^{exp}H$ for nitrogen, hydrogen fluoride, and methanol, as shown in Table 3. Some trends concerning the performance of various methods can be observed in this comparison. For dispersion-bound crystals of noble gases, many-body expansion methods are not limited by the embedding scheme, and when coupled with the gold standard CCSD(T)/CBS electronic theory, they are capable of reaching the sub-kJ·mol^{-1} level of accuracy, superior to most of the periodic DFT calculations. This partially holds also for the remaining crystals of nonpolar molecules. With an increasing significance of the electrostatic interactions, selection of an appropriate embedding scheme becomes more important, which can be illustrated by the mentioned failures of our simple point-charge model, largely neglecting three-body induction contributions. However, fragment-based computational models accounting for the long-range and many-body effects in a more sophisticate way can yield accurate cohesive energies, as reported for carbon dioxide[24,79] and formamide.[24] As expected, it is rightful to expect high accuracy from dispersion-corrected periodic DFT calculations for crystals of highly polar molecules, some of them often yielding results in closest agreement with experiment [see Tables 3 and S3 (Supporting Information)], even though no particular DFT functional seems to be superior to the others in terms of accuracy. By averaging $|\sigma_H|$ calculated for several popular functionals, the following mean $|\sigma_H|$ values were obtained: 9% for PBE-D3, 11% for vdW-DF2, and 17% for PBE-TS. Such values were, however, obtained over very limited subsets of a few crystals with available data, and moreover, they can be slightly blurred by the presence of the zero-point vibrational terms contributing to $\Delta_{sub}^{calc}H$. Periodic local MP2 calculations in their pure uncorrected form usually do not yield $\Delta_{sub}^{calc}H$ reaching the quality of DFT results. However, including some form of spin-component scaling[76] or incremental ab initio corrections[25] can improve the agreement of local MP2 results with experiment, making the latter a very promising ab initio method for evaluation of highly accurate $\Delta_{sub}H$, even though the method is currently rather cost-prohibitive for larger systems.

Selecting the literature E_{coh}^{cr} values leading to the best agreement of $\Delta_{sub}^{calc}H$ with $\Delta_{sub}^{exp}H$ experiment for the whole subset of crystals represents a way to make an optimistic estimate of the contemporary limits of ab initio chemistry in the field of predictions of $\Delta_{sub}^{calc}H$. Averaging such optimistic cases over the crystal subset yields $|\sigma_H|$ = 3%, which can be taken as the lower-bound for the computational uncertainty of $\Delta_{sub}^{calc}H$, being less than a third of the $|\sigma_H|$ obtained for $\Delta_{sub}^{calc}H$ based purely on E_{coh}^{cr} calculated in our work.[17] In this optimistic

DOI: 10.1021/acs.jctc.7b00164
J. Chem. Theory Comput. 2017, 13, 2840−2850

scenario, $\Delta_{sub}^{calc}H$ differs from $\Delta_{sub}^{exp}H$ by less than 1 kJ·mol^{-1} for 9 out of the 12 crystals and by less than 1 kcal·mol^{-1} for all 12 crystals. Furthermore, the best values of $\Delta_{sub}^{calc}H$ range within the experimental uncertainty of $\Delta_{sub}^{exp}H$, given by their expanded uncertainty (coverage factor k = 2), in 8 out of 12 cases. This means that the level of the chemical accuracy of $\Delta_{sub}^{calc}H$ calculated from first principles is reachable. However, taking into account that these optimistic cases represent a whole variety of quantum chemical methods used for calculations of E_{coh}^{cr}, including modifications of ab initio many-body expansion methods,[17,68] periodic local MP2,[71,76] and DFT calculations with periodic boundary conditions,[29,62,73,77] it cannot be granted that using a single given computational method will always result in such an optimistic case.

Concerning the comparison of $\Delta_{sub}^{calc}H$ calculated using the rigorous way based on evaluation of individual terms from eq 1 and $\Delta_{sub}^{est}H$ estimated by the "2RT" approximation, both approaches yield $\Delta_{sub}H$ of comparable accuracy, as illustrated in Figure 6, which shows all three data sets, static E_{coh}^{cr},

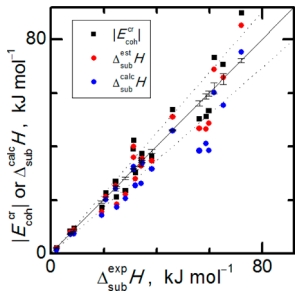

Figure 6. Comparison of $\Delta_{sub}^{exp}H$ at T_{pt} with E_{coh}^{cr} calculated at the CCSD(T)/CBS level, $\Delta_{sub}^{est}H$ estimated using the 2RT approximation, and newly calculated $\Delta_{sub}^{calc}H$ including a rigorous quasi-harmonic treatment of the thermal contributions.

estimated $\Delta_{sub}^{est}H$, and rigorously calculated $\Delta_{sub}^{calc}H$, unlike Figure 8 in our previous work,[17] which contained only data on E_{coh}^{cr} and $\Delta_{sub}^{est}H$, thus completely omitting the $\Delta_{geom}^{cr\rightarrow g}E$, $\Delta_{th,mol}^{cr\rightarrow g}E$, $\Delta_{ZPE}^{cr\rightarrow g}E$ terms and only partially accounting for the $H_{therm}^{lattice}$ term from eq 1. Since E_{coh}^{cr} dominates the total $\Delta_{sub}H$, no dramatic changes could be expected between the $\Delta_{sub}^{est}H$ and $\Delta_{sub}^{calc}H$ data sets. Since E_{coh}^{cr} is often underestimated by the ab initio calculations and the 2RT correction is usually lower in absolute value than the sum of vibrational and thermal contributions to $\Delta_{sub}H$, applying the 2RT approximation can lead to not so underestimated $\Delta_{sub}H$ values in many cases. Extreme examples of this behavior are strongly hydrogen-bound crystals of formic acid or hydrazine. This behavior cannot be explained by any physical background but by a fortuitous compensation of errors occurring when the 2RT approximation is used. From a global point of view, the proper phonon-based way should be recommended because it has a strong physical background, unlike the high-temperature limit 2RT approximation at low temperatures. Moreover, further development of DFT or ab initio phonon calculations leading to a higher accuracy of the phonon calculations, even for nonpolar molecules, is to be expected in the near future.

4. CONCLUSIONS

A rigorous computational methodology for calculations of sublimation enthalpy for molecular crystals from first principles was developed and extensively tested for a set of 22 crystals. To our knowledge, high-level theoretical calculations of the cohesive energies, phonon and thermal properties of the crystalline phases, and the thermodynamic properties of the ideal gas, including a careful analysis of the rotational and translational contributions to $C_p^{g,0}$ at very low temperatures, were combined for the first time for a broader testing set of molecular crystals. Potential performance issues of the individual building blocks forming the whole methodology were identified, and their magnitude was estimated. Highly reliable experimental data on sublimation enthalpies were used for estimating the overall computational uncertainty of sublimation enthalpies. The resulting computational uncertainty, amounting to 3% in the most optimistic cases and not exceeding 15% on average, is a promising achievement. However, for applications such as ab initio predictions of sublimation pressures, which depend on sublimation enthalpy exponentially, it cannot be accepted as accurate and reliable enough and further development of the methodology will be inevitable to cover such areas. Future development of ab initio methods should enable one to employ less costly and more accurate calculations of cohesive energies as well as the thermal properties of the crystalline phases.

■ ASSOCIATED CONTENT

Supporting Information

The Supporting Information is available free of charge on the ACS Publications website at DOI: 10.1021/acs.jctc.7b00164.

Calculated rotational temperatures, comparison of calculated and experimental sublimation enthalpies at selected temperatures, and comparison of sublimation enthalpies calculated using literature values of cohesive energies (PDF)

■ AUTHOR INFORMATION

Corresponding Author

*E-mail: cervinkc@vscht.cz.

ORCID

Ctirad Červinka: 0000-0003-1498-6715

Funding

The authors acknowledge financial support from the Czech Science Foundation (GACR No. 17-03875S). The access to computing and storage facilities owned by parties and projects contributing to the National Grid Infrastructure MetaCentrum, provided under the program "Projects of Large Infrastructure for Research, Development, and Innovations" (LM2010005) and the CERIT-SC under the program Centre CERIT Scientific Cloud, part of the Operational Program Research and Development for Innovations, Reg. No. CZ.1.05/3.2.00/08.0144, is highly appreciated.

Notes

The authors declare no competing financial interest.

■ REFERENCES

(1) Fulem, M.; Růžička, K.; Červinka, C.; Rocha, M. A. A.; Santos, L. M. N. B. F.; Berg, R. F. Recommended Vapor Pressure and Thermophysical Data for Ferrocene. *J. Chem. Thermodyn.* **2013**, *57*, 530−540.

(2) Růžička, K.; Fulem, M.; Červinka, C. Recommended Sublimation Pressure and Enthalpy of Benzene. *J. Chem. Thermodyn.* **2014**, *68*, 40−47.

DOI: 10.1021/acs.jctc.7b00164
J. Chem. Theory Comput. 2017, 13, 2840−2850

(3) Růžička, K.; Fulem, M.; Růžička, V. Recommended Vapor Pressure of Solid Naphthalene. *J. Chem. Eng. Data* **2005**, *50*, 1956−1970.
(4) Bidleman, T. F. Estimation of Vapor-Pressures for Nonpolar Organic-Compounds by Capillary Gas-Chromatography. *Anal. Chem.* **1984**, *56*, 2490−2496.
(5) Delle Site, A. The Vapor Pressure of Environmentally Significant Organic Chemicals: A Review of Methods and Data at Ambient Temperature. *J. Phys. Chem. Ref. Data* **1997**, *26*, 157−193.
(6) Růžička, K.; Koutek, B.; Fulem, M.; Hoskovec, M. Indirect Determination of Vapor Pressures by Capillary Gas-Liquid Chromatography: Analysis of the Reference Vapor-Pressure Data and Their Treatment. *J. Chem. Eng. Data* **2012**, *57*, 1349−1368.
(7) Gharagheizi, F. A New Molecular-Based Model for Prediction of Enthalpy of Sublimation of Pure Components. *Thermochim. Acta* **2008**, *469*, 8−11.
(8) McDonagh, J. L.; Palmer, D. S.; van Mourik, T.; Mitchell, J. B. O. Are the Sublimation Thermodynamics of Organic Molecules Predictable? *J. Chem. Inf. Model.* **2016**, *56*, 2162−2179.
(9) Groom, C. R.; Bruno, I. J.; Lightfoot, M. P.; Ward, S. C. The Cambridge Structural Database. *Acta Crystallogr., Sect. B: Struct. Sci., Cryst. Eng. Mater.* **2016**, *72*, 171−179.
(10) Dunitz, J. D.; Gavezzotti, A. How Molecules Stick Together in Organic Crystals: Weak Intermolecular Interactions. *Chem. Soc. Rev.* **2009**, *38*, 2622−2633.
(11) Price, S. L.; Braun, D. E.; Reutzel-Edens, S. M. Can Computed Crystal Energy Landscapes Help Understand Pharmaceutical Solids? *Chem. Commun.* **2016**, *52*, 7065−7077.
(12) Deringer, V. L.; Stoffel, R. P.; Dronskowski, R. Thermochemical Ranking and Dynamic Stability of TeO2 Polymorphs from Ab Initio Theory. *Cryst. Growth Des.* **2014**, *14*, 871−878.
(13) Heit, Y. N.; Beran, G. J. O. How Important Is Thermal Expansion for Predicting Molecular Crystal Structures and Thermochemistry at Finite Temperatures? *Acta Crystallogr., Sect. B: Struct. Sci., Cryst. Eng. Mater.* **2016**, *72*, 514−529.
(14) Hirata, S.; Gilliard, K.; He, X.; Li, J.; Sode, O. Ab Initio Molecular Crystal Structures, Spectra, and Phase Diagrams. *Acc. Chem. Res.* **2014**, *47*, 2721−2730.
(15) Li, J.; Sode, O.; Voth, G. A.; Hirata, S. A Solid-Solid Phase Transition in Carbon Dioxide at High Pressures and Intermediate Temperatures. *Nat. Commun.* **2013**, *4*, 2647.
(16) Beran, G. J. O.; Nanda, K. Predicting Organic Crystal Lattice Energies with Chemical Accuracy. *J. Phys. Chem. Lett.* **2010**, *1*, 3480−3487.
(17) Červinka, C.; Fulem, M.; Růžička, K. CCSD(T)/CBS Fragment-Based Calculations of Lattice Energy of Molecular Crystals. *J. Chem. Phys.* **2016**, *144*, 064505.
(18) Gavezzotti, A. In *Advanced X-ray Crystallography*; Rissanen, K., Ed.; Springer: Berlin, 2012; p 1.
(19) Ringer, A. L.; Sherrill, C. D. First Principles Computation of Lattice Energies of Organic Solids: the Benzene Crystal. *Chem. - Eur. J.* **2008**, *14*, 2542−2547.
(20) Yang, J.; Hu, W. F.; Usvyat, D.; Matthews, D.; Schutz, M.; Chan, G. K. L. Ab Initio Determination of the Crystalline Benzene Lattice Energy to Sub-kilojoule/mol Accuracy. *Science* **2014**, *345*, 640−643.
(21) Civalleri, B.; Doll, K.; Zicovich-Wilson, C. M. Ab Initio Investigation of Structure and Cohesive Energy of Crystalline Urea. *J. Phys. Chem. B* **2007**, *111*, 26−33.
(22) Grimme, S.; Antony, J.; Ehrlich, S.; Krieg, H. A Consistent and Accurate Ab Initio Parametrization of Density Functional Dispersion Correction (DFT-D) for the 94 Elements H-Pu. *J. Chem. Phys.* **2010**, *132*, 154104.
(23) Müller, C.; Usvyat, D.; Stoll, H. Local Correlation Methods for Solids: Comparison of Incremental and Periodic Correlation Calculations for the Argon FCC Crystal. *Phys. Rev. B: Condens. Matter Mater. Phys.* **2011**, *83*, 245136.
(24) Wen, S. H.; Beran, G. J. O. Accurate Molecular Crystal Lattice Energies from a Fragment QM/MM Approach with On-the-Fly Ab Initio Force Field Parametrization. *J. Chem. Theory Comput.* **2011**, *7*, 3733−3742.
(25) Müller, C.; Usvyat, D. Incrementally Corrected Periodic Local MP2 Calculations: I. The Cohesive Energy of Molecular Crystals. *J. Chem. Theory Comput.* **2013**, *9*, 5590−5598.
(26) Bučko, T.; Hafner, J.; Lebegue, S.; Angyan, J. G. Improved Description of the Structure of Molecular and Layered Crystals: Ab Initio DFT Calculations with van der Waals Corrections. *J. Phys. Chem. A* **2010**, *114*, 11814−11824.
(27) Carter, D. J.; Rohl, A. L. Benchmarking Calculated Lattice Parameters and Energies of Molecular Crystals Using van der Waals Density Functionals. *J. Chem. Theory Comput.* **2014**, *10*, 3423−3437.
(28) Huang, Y. H.; Shao, Y. H.; Beran, G. J. O. Accelerating MP2C Dispersion Corrections for Dimers and Molecular Crystals. *J. Chem. Phys.* **2013**, *138*, 224112.
(29) Otero-de-la-Roza, A.; Johnson, E. R. A Benchmark for Non-Covalent Interactions in Solids. *J. Chem. Phys.* **2012**, *137*, 054103.
(30) Řezáč, J.; Hobza, P. Describing Noncovalent Interactions beyond the Common Approximations: How Accurate Is the "Gold Standard," CCSD(T) at the Complete Basis Set Limit? *J. Chem. Theory Comput.* **2013**, *9*, 2151−2155.
(31) Halkier, A.; Helgaker, T.; Jorgensen, P.; Klopper, W.; Koch, H.; Olsen, J.; Wilson, A. K. Basis-Set Convergence in Correlated Calculations on Ne, N-2, and H2O. *Chem. Phys. Lett.* **1998**, *286*, 243−252.
(32) Heit, Y. N.; Nanda, K. D.; Beran, G. J. O. Predicting Finite-Temperature Properties of Crystalline Carbon Dioxide from First Principles with Quantitative Accuracy. *Chem. Sci.* **2016**, *7*, 246−255.
(33) Deringer, V. L.; Stoffel, R. P.; Dronskowski, R. Vibrational and Thermodynamic Properties of GeSe in the Quasiharmonic Approximation. *Phys. Rev. B: Condens. Matter Mater. Phys.* **2014**, *89*, 094303.
(34) Stoffel, R. P.; Wessel, C.; Lumey, M.-W.; Dronskowski, R. Ab Initio Thermochemistry of Solid-State Materials. *Angew. Chem., Int. Ed.* **2010**, *49*, 5242−5266.
(35) Irikura, K. K.; Frurip, D. J. *Computational Thermochemistry: Prediction and Estimation of Molecular Thermodynamics*; American Chemical Society: Washington, DC, 1998.
(36) Pfaendtner, J.; Yu, X.; Broadbelt, L. J. The 1-D Hindered Rotor Approximation. *Theor. Chem. Acc.* **2007**, *118*, 881−898.
(37) McQuarrie, D. A. *Statistical Mechanics*; University Science Books: Sausalito, CA, 2000.
(38) Červinka, C.; Fulem, M.; Stoffel, R. P.; Dronskowski, R. Thermodynamic Properties of Molecular Crystals Calculated within the Quasi-Harmonic Approximation. *J. Phys. Chem. A* **2016**, *120*, 2022−2034.
(39) Heit, Y.; Beran, G. J. O. Exploiting Space-Group Symmetry in Fragment-Based Molecular Crystal Calculations. *J. Comput. Chem.* **2014**, *35*, 2205−2214.
(40) Becke, A. D. Density-Functional Thermochemistry. 3. The Role of Exact Exchange. *J. Chem. Phys.* **1993**, *98*, 5648−5652.
(41) Lee, C. T.; Yang, W. T.; Parr, R. G. Development of the Colle-Salvetti Correlation-Energy Formula into a Functional of the Electron-Density. *Phys. Rev. B: Condens. Matter Mater. Phys.* **1988**, *37*, 785−789.
(42) Granatier, J.; Pitonak, M.; Hobza, P. Accuracy of Several Wave Function and Density Functional Theory Methods for Description of Noncovalent Interaction of Saturated and Unsaturated Hydrocarbon Dimers. *J. Chem. Theory Comput.* **2012**, *8*, 2282−2292.
(43) Werner, H.-J.; Knowles, P. J.; Knizia, G.; Manby, F. R.; Schütz, M. Molpro: A General-Purpose Quantum Chemistry Program Package. *Wiley Interdisciplinary Reviews: Computational Molecular Science* **2012**, *2*, 242−253.
(44) Frisch, M. J.; Trucks, G. W.; Schlegel, H. B.; Scuseria, G. E.; Robb, M. A.; Cheeseman, J. R.; Montgomery, J. A., Jr.; Vreven, T.; Kudin, K. N.; Burant, J. C.; Millam, J. M. I., S, S.; Tomasi, J.; Barone, V.; Mennucci, B.; Cossi, M.; Scalmani, G.; Rega, N.; Petersson, G. A.; Nakatsuji, H.; Hada, M.; Ehara, M.; Toyota, K.; Fukuda, R.; Hasegawa, J.; Ishida, M.; Nakajima, T.; Honda, Y.; Kitao, O.; Nakai, H.; Klene, M.; Li, X.; Knox, J. E.; Hratchian, H. P.; Cross, J. B.; Bakken, V.; Adamo, C.; Jaramillo, J.; Gomperts, R.; Stratmann, R. E.; Yazyev, O.;

DOI: 10.1021/acs.jctc.7b00164
J. Chem. Theory Comput. 2017, 13, 2840−2850

Austin, A. J.; Cammi, R.; Pomelli, C.; Ochterski, J. W.; Ayala, P. Y.; Morokuma, K.; Voth, G. A.; Salvador, P.; Dannenberg, J. J.; Zakrzewski, V. G.; Dapprich, S.; Daniels, A. D.; Strain, M. C.; Farkas, O.; Malick, D. K.; Rabuck, A. D.; Raghavachari, K.; Foresman, J. B.; Ortiz, J. V.; Cui, Q.; Baboul, A. G.; Clifford, S.; Cioslowski, J.; Stefanov, B. B.; Liu, G.; Liashenko, A.; Piskorz, P.; Komaromi, I.; Martin, R. L.; Fox, D. J.; Keith, T.; Al-Laham, M. A.; Peng, C. Y.; Nanayakkara, A.; Challacombe, M.; Gill, P. M. W.; Johnson, B.; Chen, W.; Wong, M. W.; Gonzalez, C.; Pople, J. A. *Gaussian 03*; Gaussian, Inc.: Wallingford, 2004.

(45) Blöchl, P. E. Projector Augmented-Wave Method. *Phys. Rev. B: Condens. Matter Mater. Phys.* **1994**, *50*, 17953−17979.

(46) Klimeš, J.; Bowler, D. R.; Michaelides, A. Chemical Accuracy for the Van Der Waals Density Functional. *J. Phys.: Condens. Matter* **2010**, *22*, 022201.

(47) Hafner, J.; Kresse, G.; Vogtenhuber, D.; Marsman, M. *VASP*; 2014.

(48) Monkhorst, H. J.; Pack, J. D. Special Points for Brillouin-Zone Integrations. *Phys. Rev. B* **1976**, *13*, 5188−5192.

(49) Parlinski, K.; Li, Z. Q.; Kawazoe, Y. First-Principles Determination of the Soft Mode in Cubic ZrO2. *Phys. Rev. Lett.* **1997**, *78*, 4063−4066.

(50) Togo, A. *Phonopy*; 2009.

(51) Murnaghan, F. D. The Compressibility of Media under Extreme Pressures. *Proc. Natl. Acad. Sci. U. S. A.* **1944**, *30*, 244−247.

(52) Červinka, C.; Fulem, M.; Růžička, K. Evaluation of Accuracy of Ideal-Gas Heat Capacity and Entropy Calculations by Density Functional Theory (DFT) for Rigid Molecules. *J. Chem. Eng. Data* **2012**, *57*, 227−232.

(53) Pitzer, K. S. Energy Levels and Thermodynamic Functions for Molecules with Internal Rotation 0.2. Unsymmetrical Tops Attached to a Rigid Frame. *J. Chem. Phys.* **1946**, *14*, 239−243.

(54) Pitzer, K. S.; Gwinn, W. D. Energy Levels and Thermodynamic Functions for Molecules with Internal Rotation I. Rigid Frame with Attached Tops. *J. Chem. Phys.* **1942**, *10*, 428−440.

(55) Marston, C. C.; Balint-Kurti, G. G. The Fourier Grid Hamiltonian Method for Bound-State Eigenvalues and Eigenfunctions. *J. Chem. Phys.* **1989**, *91*, 3571−3576.

(56) Fulem, M.; Růžička, K.; Červinka, C.; Bazyleva, A.; Della Gatta, G. Thermodynamic Study of Alkane-Alpha,Omega-Diamines - Evidence of Odd-Even Pattern of Sublimation Properties. *Fluid Phase Equilib.* **2014**, *371*, 93−105.

(57) Wilson, E. B. The Statistical Weights of the Rotational Levels of Polyatomic Molecules, Including Methane, Ammonia, Benzene, Cyclopropane and Ethylene. *J. Chem. Phys.* **1935**, *3*, 276−285.

(58) Perdew, J. P.; Burke, K.; Ernzerhof, M. Generalized Gradient Approximation Made Simple. *Phys. Rev. Lett.* **1996**, *77*, 3865−3868.

(59) Červinka, C.; Fulem, M.; Růžička, K. Evaluation of Uncertainty of Ideal-Gas Entropy and Heat Capacity Calculations by Density Functional Theory (DFT) for Molecules Containing Symmetrical Internal Rotors. *J. Chem. Eng. Data* **2013**, *58*, 1382−1390.

(60) Červinka, C.; Fulem, M.; Štejfa, V.; Růžička, K. Analysis of Uncertainty in the Calculation of Ideal-Gas Thermodynamic Properties Using the One-Dimensional Hindered Rotor (1-DHR) Model. *J. Chem. Eng. Data* **2017**, *62*, 445−455.

(61) East, A. L. L.; Radom, L. Ab Initio Statistical Thermodynamical Models for the Computation of Third-Law Entropies. *J. Chem. Phys.* **1997**, *106*, 6655−6674.

(62) Moellmann, J.; Grimme, S. DFT-D3 Study of Some Molecular Crystals. *J. Phys. Chem. C* **2014**, *118*, 7615−7621.

(63) Feistel, R.; Wagner, W. Sublimation Pressure and Sublimation Enthalpy of H2O Ice Ih between 0 and 273.16 K. *Geochim. Cosmochim. Acta* **2007**, *71*, 36−45.

(64) Azreg-Ainou, M. Low-Temperature Data for Carbon Dioxide. *Monatsh. Chem.* **2005**, *136*, 2017−2027.

(65) Al-Saidi, W. A.; Voora, V. K.; Jordan, K. D. An Assessment of the vdW-TS Method for Extended Systems. *J. Chem. Theory Comput.* **2012**, *8*, 1503−1513.

(66) Harl, J.; Kresse, G. Cohesive energy curves for noble gas solids calculated by adiabatic connection fluctuation-dissipation theory. *Phys. Rev. B: Condens. Matter Mater. Phys.* **2008**, *77*, 045136.

(67) Nolan, S. J.; Bygrave, P. J.; Allan, N. L.; Manby, F. R. Comparison of the Incremental and Hierarchical Methods for Crystalline Neon. *J. Phys.: Condens. Matter* **2010**, *22*, 074201.

(68) Rosciszewski, K.; Paulus, B.; Fulde, P.; Stoll, H. Ab Initio Coupled-Cluster Calculations for the FCC and HCP Structures of Rare-Gas Solids. *Phys. Rev. B: Condens. Matter Mater. Phys.* **2000**, *62*, 5482−5488.

(69) Sansone, G.; Civalleri, B.; Usvyat, D.; Toulouse, J.; Sharkas, K.; Maschio, L. Range-separated double-hybrid density-functional theory applied to periodic systems. *J. Chem. Phys.* **2015**, *143*, 102811.

(70) Lotrich, V. F.; Szalewicz, K. Three-body Contribution to Binding Energy of Solid Argon and Analysis of Crystal Structure. *Phys. Rev. Lett.* **1997**, *79*, 1301−1304.

(71) Maschio, L.; Usvyat, D.; Civalleri, B. Ab Initio Study of Van Der Waals and Hydrogen-Bonded Molecular Crystals with a Periodic Local-MP2Method. *CrystEngComm* **2010**, *12*, 2429−2435.

(72) Bordner, A. J. Assessing the Accuracy of SAPT(DFT) Interaction Energies by Comparison with Experimentally Derived Noble Gas Potentials and Molecular Crystal Lattice Energies. *ChemPhysChem* **2012**, *13*, 3981−3988.

(73) Civalleri, B.; Zicovich-Wilson, C. M.; Valenzano, L.; Ugliengo, P. B3LYP Augmented with An Empirical Dispersion Term (B3LYP-D*) as Applied to Molecular Crystals. *CrystEngComm* **2008**, *10*, 405−410.

(74) Brandenburg, J. G.; Grimme, S. Accurate Modeling of Organic Molecular Crystals by Dispersion-Corrected Density Functional Tight Binding (DFTB). *J. Phys. Chem. Lett.* **2014**, *5*, 1785−1789.

(75) Klimeš, J. Lattice Energies of Molecular Solids from the Random Phase Approximation with Singles Corrections. *J. Chem. Phys.* **2016**, *145*, 094506.

(76) Maschio, L.; Usvyat, D.; Schutz, M.; Civalleri, B. Periodic Local Møller-Plesset Second Order Perturbation Theory Method Applied to Molecular Crystals: Study of Solid NH3 and CO2 Using Extended Basis Sets. *J. Chem. Phys.* **2010**, *132*, 134706.

(77) Reilly, A. M.; Tkatchenko, A. Understanding the Role of Vibrations, Exact Exchange, and Many-body van der Waals Interactions in the Cohesive Properties of Molecular Crystals. *J. Chem. Phys.* **2013**, *139*, 024705.

(78) Sharkas, K.; Toulouse, J.; Maschio, L.; Civalleri, B. Double-Hybrid Density-Functional Theory Applied to Molecular Crystals. *J. Chem. Phys.* **2014**, *141*, 044105.

(79) Bygrave, P. J.; Allan, N. L.; Manby, F. R. The Embedded Many-body Expansion for Energetics of Molecular Crystals. *J. Chem. Phys.* **2012**, *137*, 164102.

(80) Sode, O.; Hirata, S. Second-Order Many-Body Perturbation Study of Solid Hydrogen Fluoride. *J. Phys. Chem. A* **2010**, *114*, 8873−8877.

(81) Nagayoshi, K.; Kitaura, K.; Koseki, S.; Re, S. Y.; Kobayashi, K.; Choe, Y. K.; Nagase, S. Calculation of Packing Structure of Methanol Solid Using Ab Initio Lattice Energy at the MP2 Level. *Chem. Phys. Lett.* **2003**, *369*, 597−604.

DOI: 10.1021/acs.jctc.7b00164
J. Chem. Theory Comput. 2017, 13, 2840−2850